11th World Congress on Computational Mechanics (WCCM XI)
5th European Conference on Computational Mechanics (ECCM V)
6th European Conference on Computational Fluid Dynamics (ECFD VI)
E. Oñate, J. Oliver and A. Huerta (Eds)

A HYBRID MESH LINEAR HARMONIC SOLVER FOR THE AEROELASTIC ANALYSIS OF TURBOMACHINERY

CHRISTIAN FREY, HANS-PETER KERSKEN

German Aerospace Center (DLR), Institute of Propulsion Technology
Linder Höhe, 51147 Cologne, Germany
Christian.Frey@dlr.de, Hans-Peter.Kersken@dlr.de

Key words: Time-linearised Methods, Frequency Domain Solvers, Aeroelasticity, Turbomachinery.

Abstract. This paper describes the main ingredients of an efficient simulation tool for blade flutter in turbomachinery. The unsteady flow is modelled by the linear harmonic equations. Special emphasis is put on the extension of existing CFD methods for unstructured mesh topologies and non-matching block interfaces.

INTRODUCTION

This paper describes the implementation of a solver for the linearised three-dimensional, Reynolds-averaged Navier-Stokes equation in the frequency domain on structured and unstructured meshes. Linear harmonic methods are particularly attractive to simulate blade flutter in turbomachinery. In order to apply linear techniques to complex configurations, e.g., computational domains with cavities as shown in Fig. 1, the authors extend an existing solver which, on the one hand, provides a structured linearised solver module [8], [3], and, on the other hand, a non-linear solver for *hybrid* meshes, i.e., meshes which decompose into structured and unstructured blocks [16].

The linear harmonic (sometimes called *time-linearised*) approach [5] consists in linearising of the unsteady flow equation around a steady solution and formulating the system in the frequency domain, which results in a complex linear equation for each angular frequency.

In the first sections of this paper we outline the main ingredients of an efficient tool chain for turbomachinery flutter simulations. This includes a preprocess tool for mesh deformations but also crucial CFD solver features such as nonreflecting boundary conditions. These methods have been implemented by the authors in DLR's simulation code for internal flow, TRACE, [15, 8, 3]. However, previous publications all referred to implementations for structured meshes.

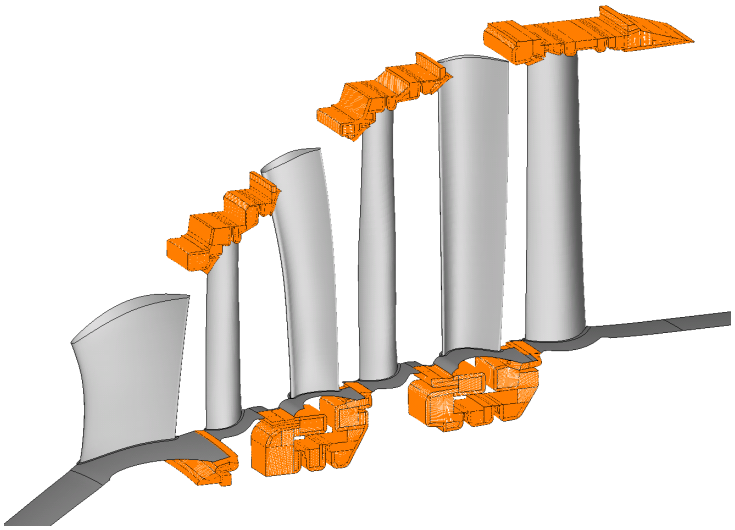

Figure 1: Turbine configuration with cavities.

Therefore, the main purpose of this work is to describe the extension of the above methods for hybrid meshes, i.e., of meshed which can be decomposed into structured and unstructured blocks. In particular, we show how to compute and store the flux Jacobians involved. It is verified that the resulting time-linearised unstructured solver is indeed of second order spatial accuracy. Another key ingredient necessary to mesh geometry details such as cavities in turbomachinery are unstructured block cuts. Their treatment in the linearised solver is outlined.

1 LINEAR HARMONIC FLOW EQUATIONS

The CFD code under consideration solves the Reynolds-averaged Navier-Stokes equations on so-called *hybrid* meshes using domain decomposition, i.e., the computational grids consist of structured and unstructured blocks. The parallelisation uses MPI to communicate flow states in neighbouring blocks to so-called ghost cells.

In analogy to the so-called *discrete adjoint* methodology [10] the linearisation approach applied here can be termed *discrete linear*. More precisely, we do not discretise the linearised flow equations but linearise the discrete URANS equations implemented in the nonlinear time-domain solver,

$$\frac{dq}{dt} + R(t, q(t)) = 0. \tag{1}$$

The underlying flow solver is based on the finite volume approach, i.e., the residual in the i-th cell is defined as

$$R_i = \frac{1}{V_i} \sum_{\sigma \in c_i} F_\sigma(q) - S_i(q) \tag{2}$$

where appropriate numerical flux functions F_σ are defined for each face. Since the flow equations are formulated in the relative system, rotational source terms appear which are denoted by S_i. Here, q is the vector of conservative variables and t denotes the physical time. Assuming that the unsteady flow is the perturbation of a steady flow by a harmonic disturbance with angular frequency ω, we may approximate the solution by

$$q(t) = \widehat{q}_0 + \mathrm{Re}\left[\widehat{q}_\omega e^{\mathbf{i}\omega t}\right], \tag{3}$$

cf. [2, 8]. Under the assumption that the amplitudes $|\widehat{q}_\omega|$ are small, one may approximate R by its linearisation, i.e.

$$R(q(t)) \approx \frac{\partial R}{\partial q}\,\mathrm{Re}\left[\widehat{q}_\omega e^{\mathbf{i}\omega t}\right] = \mathrm{Re}\left[\frac{\partial R}{\partial q}\widehat{q}_\omega e^{\mathbf{i}\omega t}\right]. \tag{4}$$

Here, we have used the fact that the time-average $\widehat{q}_0$ is an approximate solution to the steady equations, i.e.

$$R(\widehat{q}_0) \approx 0.$$

We infer,

$$\Big(\mathbf{i}\omega + \frac{\partial R}{\partial q}\Big)\widehat{q}_\omega = 0. \tag{5}$$

These so-called *time-linearised* flow equations are particularly appealing for applications where:

- The unsteady perturbations are small, therefore the linearisation error is expected to be acceptable.
- One is interested in one (or a few) frequencies only, so the full temporal resolution of a period is unnecessary.

2 BOUNDARY CONDITIONS

On the one hand, the solution problem for Eqn. (5) is less complex than the integration of the unsteady system in Eqn. (1). However, a further advantage of frequency domain methods is that phase-lagged periodic boundary conditions and non-reflecting boundary conditions can be implemented directly in the frequency domain. These two boundary conditions are essential for unsteady simulations of turbomachinery flows. Their implementation constitutes a challenging problem in the time domain [13, 7]; e.g. subtle approximations are neccessary to implement well-posed non-reflecting boundary conditions in the time domain [4].

In the frequency domain, the phase-lagged periodicity condition reads

$$\widehat{q}_\omega(\theta + \Delta\theta) = e^{\mathbf{i}\sigma}\widehat{q}_\omega(\theta),$$

for an interblade phase angle of σ and a pitch angle of $\Delta\theta$. Note that this is merely a slight modification of the standard periodic condition.

The implementation of nonreflecting boundary conditions here is based on the assumption that the faces at the inlet and outlet boundary can be decomposed into so-called bands, i.e., rotationally symmetric annular segments [3, 7].

3 MESH DEFORMATIONS

The standard approach to simulate turbomachinery blade flutter is to predict the unsteady flow under a prescribed blade vibration. Usually, one considers the first few eigenmodes which have been obtained from a structural mode analysis of the blade. Since the finite element grids typically use a different mesh resolution for the blade surfaces than the CFD one has to interpolate the blade eigenmodes between the grids. Once the eigenmodes are mapped to the CFD surface mesh, an elliptic mesh deformation method is employed in order to obtain a corresponding grid displacement. These two process steps are part of DLR's preprocessing tool PREP [15].

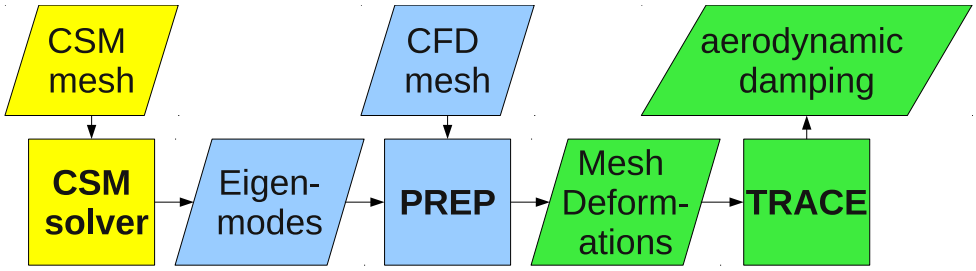

Figure 2: Process Chain for Aeroelastic Analysis.

In order to simulate flows on moving meshes the numerical flux functions are modified,

$$F'_\sigma(q, x, \dot{x}) = F_\sigma(q, x) - \dot{x}_\sigma \cdot \vec{n}_\sigma \; |\sigma| q,$$

where $\vec{n}_\sigma$ and $\dot{x}_\sigma$ denote the outward pointing normal vector and the velocity of the face σ, respectively. Given a harmonic mesh deformation

$$x(t) = \hat{x}_0 + \mathrm{Re}\left[\hat{x}_\omega e^{\mathbf{i}\omega t}\right]$$

the linear harmonic flow equations

$$\left(\mathbf{i}\omega + \frac{\partial R}{\partial q}\right)\hat{q}_\omega = -\left[\frac{\partial R}{\partial x}\hat{x}_\omega + \frac{\partial R}{\partial \dot{x}}\mathbf{i}\omega\hat{x}_\omega + \mathbf{i}\omega\frac{\hat{q}_0}{\hat{V}_0}\hat{V}_\omega\right], \tag{6}$$

are solved using the GMRES method. From the harmonic solution $\hat{q}_\omega$ one calculates the aerodynamic work, cf. [8]. Figure 2 gives an overview of the tools involved. The linear harmonic flow solver has been validated for different test cases such as the 10th standard configurations against reference solutions obtained with different solvers [11], see Figure 3. Further comparisons with reference results may be found in [8].

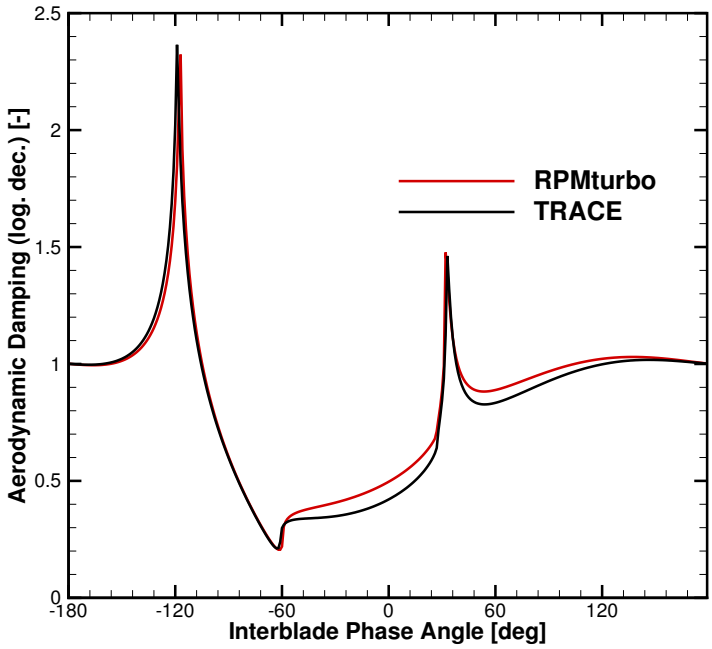

Figure 3: Aerodynamic Damping over Interblade Phase Angle for Standard Configuration 10.

4 HYBRID MESHES

One difficulty in the present approach is the linearisation of the numerical residuals, defined in Eqn. (2). These are based on the finite volume approach using Roe's upwind scheme [12] which is extended to second order accuracy using van Leer's MUSCL extrapolation technique [14] on structured blocks. Similarly, on unstructured meshes the flow gradients at cell centres are calculated using the Green Gauss formulation or least squares approximations. The flow gradients are used to extrapolate second order accurate left and right states for the Roe scheme. Furthermore, appropriate limiters for the structured and unstructured schemes are employed to prevent spurious oscillations in the vicinity of shocks.

Viscous terms are based on gradients which, in turn, are computed from second-order accurate finite differences on structured meshes, or the (unlimited) gradients on unstructured meshes, respectively. Further details may be found in [9] and [1]. Turbulence models are used to compute steady flows but are frozen in the linear harmonic mode.

Both for structured and unstructured grids the Jacobian of the residual,

$$\frac{\partial R_i}{\partial q} = \frac{1}{V_i} \sum_{\sigma \in c_i} \frac{\partial F_\sigma}{\partial q} - \frac{\partial S_i}{\partial q}, \tag{7}$$

is, apart from the source term Jacobian, essentially the weighted sum of the Jacobians of

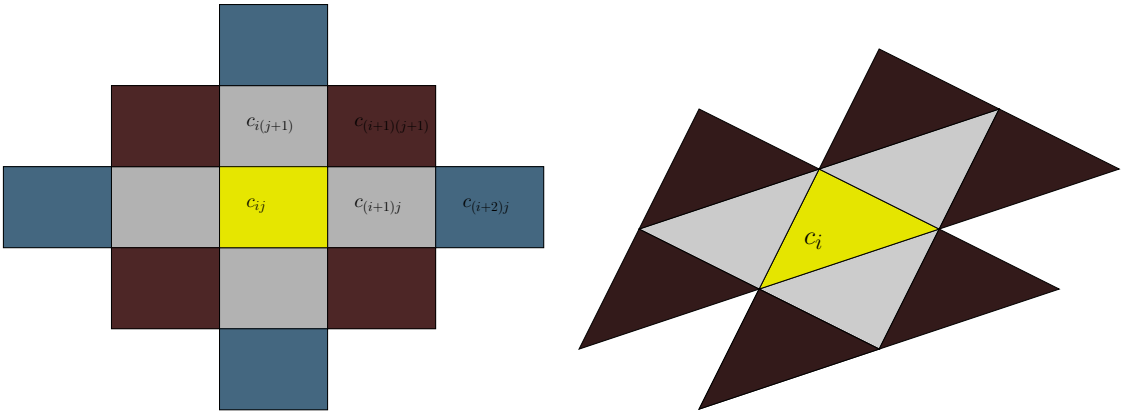

Figure 4: Stencil for the second order Navier-Stokes residual on structured (left) and unstructured (right) meshes.

convective and viscous fluxes

$$F_{\sigma,\mathrm{conv}}(q_\mathrm{L}, q_\mathrm{R}) + F_{\sigma,\mathrm{visc}}((\nabla q)_\sigma) \tag{8}$$

where the former is based on Roe's scheme. The so-called *left* and *right* states are based on second order accurate extrapolation schemes, i.e., on structured grids,

$$q_\mathrm{L} = q_i + \frac{1}{2}(\widetilde{\Delta} q)_\mathrm{L}, \quad q_\mathrm{R} = q_{i+1} - \frac{1}{2}(\widetilde{\Delta} q)_\mathrm{R} \tag{9}$$

whereas, on unstructured grids, we have

$$q_\mathrm{L} = q_i + (\widetilde{\nabla} q)_\mathrm{L} \cdot (x_\sigma - x_i), \quad q_\mathrm{R} = q_{i'} + (\widetilde{\nabla} q)_\mathrm{R} \cdot (x_\sigma - x_{i'}). \tag{10}$$

Here, $\Delta q_{\mathrm{L/R}}$ is the approximation of the derivative w.r.t. the mesh coordinate which is transversal to the face σ. $\nabla q_{\mathrm{L/R}}$ denote the cell-centred gradients. By $\widetilde{\Delta} q_{\mathrm{L/R}}$ and $\widetilde{\nabla} q_{\mathrm{L/R}}$ we denote the limited slopes and gradients, respectively [6, 1].

In the simplest form, the viscous flux is computed from cell centred gradients using interpolated face gradients, i.e.

$$(\nabla q)_\sigma = w_\mathrm{L}(\nabla q)_\mathrm{L} + w_\mathrm{R}(\nabla q)_\mathrm{R}. \tag{11}$$

Typical stencils for structured and unstructured grids are shown in Fig. 4. The neighbouring cells which are employed for a first order stencil of the inviscid fluxes are plotted in grey. The cells which are needed for the face (structured) or Gauss Green (unstructured) gradients are marked in brown. Moreover, for structured grids, the second order MUSCL extrapolation uses the cells marked in blue.

For structured meshes we build the sparse block matrix containing all residual Jacobians

$$\frac{\partial R_i}{\partial q_{i'}}. \tag{12}$$

The left diagram in Figure 4 shows the stencil in two dimensions. The i-th residual depends on cells which influence the MUSCL extrapolation and those needed for the face gradients used in the viscous flux computations. In three dimensions the stencil size is therefore 25. In order to approximate (12) on structured blocks we compute a central finite difference of the residuals w.r.t. the primitive variables in all cells of this stencil. The resulting 5×5-matrices are subsequently transformed to derivatives w.r.t. conservative variables [8]. Observe that the residual in each structured block depends on two layers of ghost cells. Therefore, in order to apply the linearised residual to a vector that corresponds to a harmonics flow field, one has to communicate two layers of interior cells and set the boundary conditions [3].

The above methodology for structured grids does not carry over to unstructured grids since the mesh topology of the remote block is unknown in the local block. In order to circumvent this problem we therefore consider the unstructured residual first as a function of the cell centres and the flow gradients in the neighbouring cells. By virtue of Eqns. (10) and (11) we approximate

$$\frac{\partial F_\sigma}{\partial q_{\mathrm{cc}}}, \quad \frac{\partial F_\sigma}{\partial (\nabla_x q)}, \quad \frac{\partial F_\sigma}{\partial (\nabla_y q)}, \quad \frac{\partial F_\sigma}{\partial (\nabla_z q)}, \tag{13}$$

again by central finite differences. Observe that this results in four sparse block matrices with a band width that corresponds to a direct neighbour stencil.

In order to apply the residual Jacobian to a harmonic flow field $\hat{q}_\omega$ four matrix vector multiplications are performed,

$$\frac{\partial R}{\partial q}\hat{q}_\omega = \frac{\partial R}{\partial q_{\mathrm{cc}}}\hat{q}_\omega + \frac{\partial R}{\partial (\nabla_x q)}\nabla_x \hat{q}_\omega + \frac{\partial R}{\partial (\nabla_y q)}\nabla_y \hat{q}_\omega + \frac{\partial R}{\partial (\nabla_z q)}\nabla_z \hat{q}_\omega. \tag{14}$$

However, in order to apply the operators on the right-hand side of Eqn. (14), the interblock communication has to be modified. First the cell centred values are communicated such

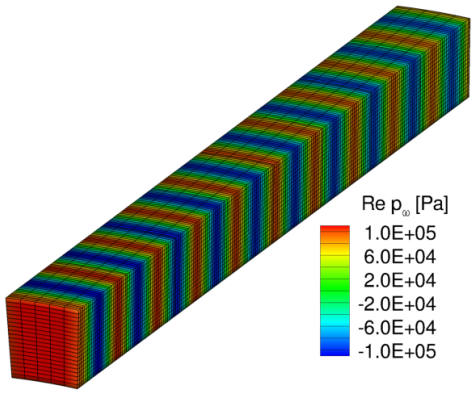

Figure 5: Harmonic solution for the measurement of numerical dissipation.

that the flow gradients in all inner cells can be computed. Then the inner flow gradients are copied to the ghost cells in a subsequent communication step.

Note that, for structured grids, the preconditioner for the GMRES solver is computed from the sparse matrix corresponding to the second order accurate spatial scheme. In contrast to this, the preconditioner for unstructured blocks is computed from $\frac{\partial R}{\partial q_{\mathrm{cc}}}$ only, which can be viewed as an inviscid first order residual Jacobian.

In order to demonstrate that the spatial discretisation order is conserved for the linearised solver, a numerical experiment is performed where a harmonic, acoustic perturbation is prescribed at the inlet of a rectangular block with constant mean flow, see Fig. 5. By varying the angular frequency of the disturbance this test is performed for different numbers of cells per wave length. The mesh is structured but is also converted into an unstructured hexahedra mesh in order to compare the structured and unstructured linear harmonic solver. The results for the first and second order spatial accuracy are plotted in Fig. 6. The comparison with reference lines of first and second order show that the design accuracy is indeed achieved. Moreover, the dissipation error of the structured discretisation seems to decrease slightly faster than that of the unstructured scheme.

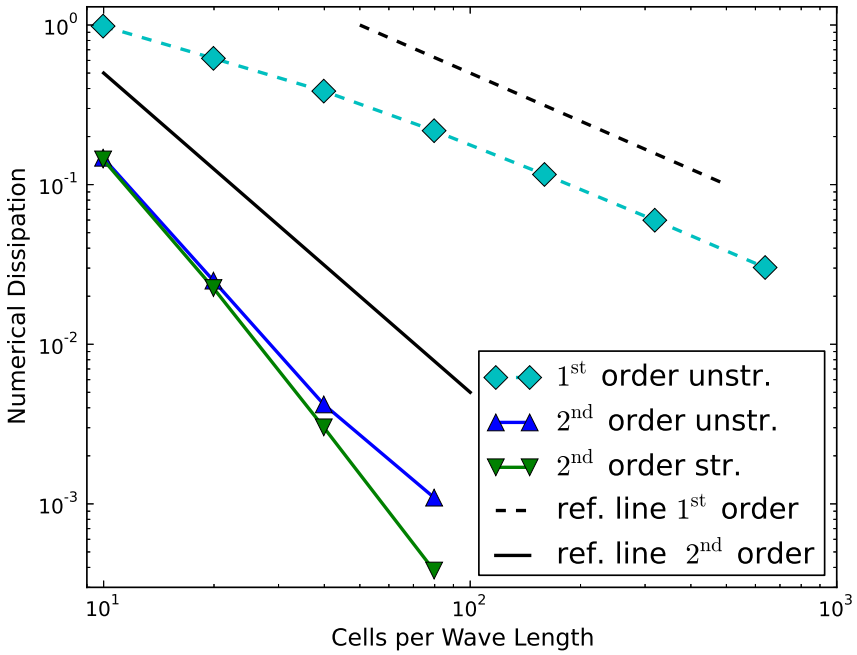

Figure 6: Numerical dissipation of the structured and unstructured scheme for a hexahedral mesh.

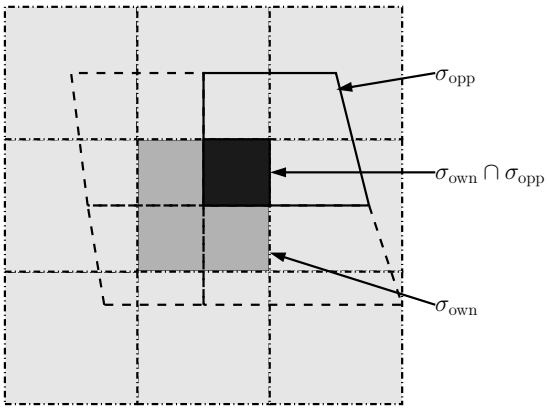

Figure 7: Clipping algorithm for non-matching block interfaces.

5 NON-MATCHING BLOCK INTERFACES

One of the key techniques developed for the hybrid mesh RANS solver is a conservative and second-order accurate coupling algorithm developed for non-matching block interfaces [17]. Figure 7 shows an example of the interface between two grids.

The first step of this coupling method is purely geometric and consists in determining which faces intersect and computing the area of the intersection, $\text{area}(\sigma_{i,\text{own}} \cap \sigma_{j,\text{opp}})$. These give rise to the interpolation weights

$$w_{ij} = \frac{\text{area}(\sigma_{i,\text{own}} \cap \sigma_{j,\text{opp}})}{\text{area}(\sigma_{i,\text{own}})}$$

In the nonlinear solver these intersection areas are then used to exchange cell centred flow states, MUSCL-extrapolated states and numerical fluxes such that the resulting scheme shares the main features with the standard scheme at inner faces. In particular, the same slope limiters, Roes upwind fluxes and central differencing formulations are applied to evaluate the convective and viscous fluxes, respectively. In order to achieve a conservative formulation the numerical fluxes are computed locally, communicated to the opposite block, interpolated using the weights w_{ij} above, and replaced with the average of local and remote fluxes.

The non-matching block interface has been implemented in the linearised solver for first order spatial accuracy only. Moreover, the viscous fluxes are based on the so-called thin shear layer approximation, i.e., the flux through a face σ depends on the neighbouring cells only. The linearisation of the cell residuals is calculated for block boundary cells in the same way as for inner cells. The harmonic flow vectors are communicated to neighbouring blocks. At non-matching block interfaces the interpolation weights w_{ij} are used to compute harmonic flow states in the ghost cells. Figure 8 shows the steady and linear harmonic solutions for the flutter analysis of a turbine blade near a non-matching

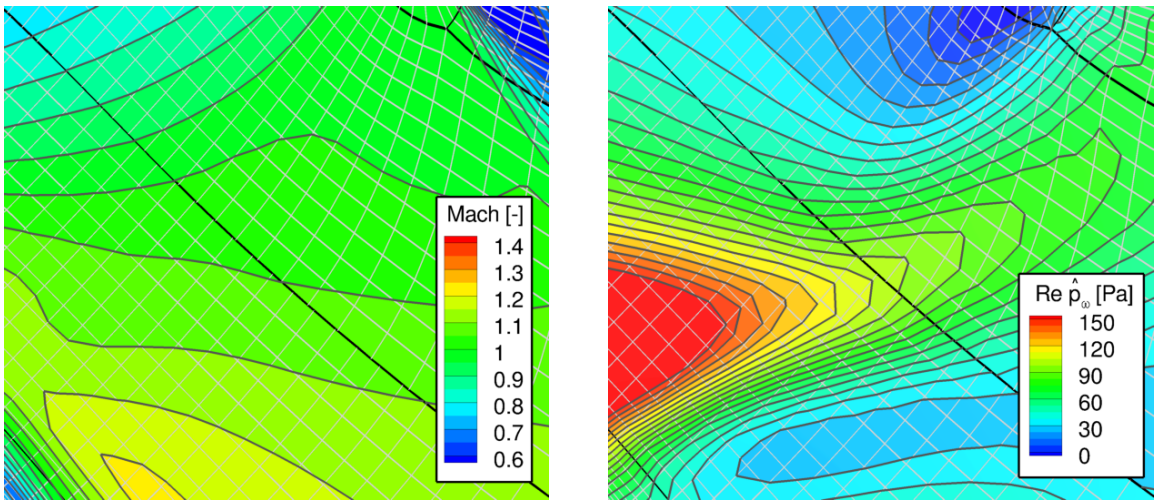

Figure 8: Mach number contours of steady solution (left) and harmonic pressure (right).

periodic block connectivity. In both cases the contour lines (dark grey lines), show that the solutions are "continuous" across the block boundaries (black lines).

SUMMARY AND CONCLUSIONS

This paper summarises the main features necessary to make efficient flutter predictions for turbomachinery blades. For this purpose the linear harmonic approach is particularly attractive since it allows for a straightforward implementation of phase-lag periodicity and nonreflecting boundary conditions, which are key features necessary to accurately simulate unsteady flows in turbomachinery.

In order to perform high fidelity simulations it is desirable to allow for an accurate and flexible meshing of geometric features such as clearances, blade fillets, bleedings, and cavities. In this paper an existing aeroelastic tool chain for turbomachinery applications is generalised in such a way that both structured and unstructured meshes can be employed. Moreover, unstructured block interface have been implemented for configurations where the meshing with one-to-one connectivities turns out to be unfeasible.

ACKNOWLEDGEMENTS

This research was supported by the German Federal Ministry of Economic Affairs and Energy under grant numbers 03ET2012G.

REFERENCES

[1] K. Becker and G. Ashcroft. A comparative study of gradient reconstruction methods for unstructured meshes with application to turbomachinery flows. In *52nd AIAA Aerospace Sciences Meeting*, National Harbor, MD, USA, Jan. 2014.

[2] W. S. Clark and K. C. Hall. A time-linearized Navier-Stokes analysis of stall flutter. *J. Turbomachinery*, 122:467–476, 2000.

[3] C. Frey, G. Ashcroft, H.-P. Kersken, and C. Weckmüller. Advanced numerical methods for the prediction of tonal noise in turbomachinery — Part II: Time-linearized methods. *Journal of Turbomachinery*, 136(2):021002–021002, 2013.

[4] M. B. Giles. Non-reflecting boundary conditions for the Euler equations. Technical report, MIT Dept. of Aero. and Astr., 1988. CFDL Report 88-1.

[5] K. C. Hall and E. F. Crawley. Calculation of unsteady flows in turbomachinery using the linearized Euler equations. *AIAA Journal*, 27(6):777–787, 1989.

[6] C. Hirsch. *Numerical Computation of Internal and External Flows – Computational Methods for Inviscid and Viscous Flows*, volume 2. Wiley, 1 edition, 1990.

[7] H.-P. Kersken, G. Ashcroft, C. Frey, N. Wolfrum, and D. Korte. Nonreflecting boundary conditions for aeroelastic analysis in time and frequency domain 3D RANS solvers. In *Proceedings of ASME Turbo Expo 2014*, 2014.

[8] H.-P. Kersken, C. Frey, C. Voigt, and G. Ashcroft. Time-Linearized and Time-Accurate 3D RANS Methods for Aeroelastic Analysis in Turbomachinery. *J. Turbomach.*, 134(5), 2012.

[9] E. Kügeler, A. Weber, and S. Lisiewicz. Combination of a transition model with a two-equation turbulence model and comparison with experimental results. In *4th European Conference of Turbomachinery*, 2001.

[10] R. M. Lewis. Numerical computation of sensitivities and the adjoint approach. In J. Borggaard, J. Burns, E. Cliff, and S. Schreck, editors, *Computational Methods for Optimal Design and Control*, pages 285–302. Birkhäuser, 1998.

[11] P. J. Petrie-Repar, A. M. McGhee, and P. A. Jacobs. Three-dimensional viscous flutter analysis of standard configuration 10. In *ASME Turbo Expo 2007: Power for Land, Sea, and Air*, 2007.

[12] P. L. Roe. Approximate Riemann solvers, parameter vectors, and difference schemes. *Journal of Computational Physics*, 43(2):357–372, 1981.

[13] R. Schnell and D. Nürnberger. Investigation of the tonal acoustic field of a transonic fanstage by time-domain CFD-calculation with arbitrary blade counts. In *ASME-Paper*, 2004.

[14] B. van Leer. Towards the ultimate conservative difference scheme. V. a second-order sequel to Godunov's method. *Journal of Computational Physics*, 32(1):101–136, 1979.

[15] C. Voigt, C. Frey, and H.-P. Kersken. Development of a generic surface mapping algorithm for fluid-structure-interaction simulations in turbomachinery. In J. C. F. Pereira, A. Sequeira, and J. M. C. Pereira, editors, *V European Conference on Computational Fluid Dynamics ECCOMAS CFD 2010*, June 2010.

[16] H. Yang, D. Nürnberger, and H.-P. Kersken. Towards excellence in turbomachinery computational fluid dynamics. *Journal of Turbomachinery*, 2006(128):390–402, 2006.

[17] H. Yang, D. Nürnberger, E. Nicke, and A. Weber. Numerical investigation of casing treatment mechanisms with a conservative mixed-cell approach. In *ASME IGTI*, 2003. Paper-No. 2003-GT-38483.